Available online at www.sciencedirect.com
ScienceDirect
Journal of the European Ceramic Society 31 (2011) 1353–1360
www.elsevier.com/locate/jeurceramsoc

The role of firing temperature, firing time and quartz grain size on phase-formation, thermal dilatation and water absorption in sanitary-ware vitreous bodies

A. Bernasconi [a], V. Diella [b,*], A. Pagani [b], A. Pavese [a,b], F. Francescon [c], K. Young [d], J. Stuart [d], L. Tunnicliffe [d]

[a] *Dipartimento di Scienze della Terra, Università di Milano, Via Botticelli 23, I-20133 Milano, Italy*
[b] *National Research Council, IDPA, Section of Milan, Via Botticelli 23, I-20133 Milano, Italy*
[c] *Ideal Standard International, C.O.E., Ceramic Process Technology, Via Cavassico Inferiore 160, I-32026 Trichiana (BL), Italy*
[d] *SIBELCO, Group Central Laboratory, Moneystone Quarry, Whiston, Stoke-on-Trent ST10 2DZ, United Kingdom*

Received 18 November 2010; received in revised form 21 January 2011; accepted 3 February 2011

Abstract

This work reports a study on (i) the evolution of mineral phases versus time and temperature, and (ii) some relationships between phases observed, process parameters, and macroscopic properties (thermal expansion and water absorption), in sanitary-ware vitreous bodies. These properties are relevant to satisfying the technical requirements of sanitary-ware. We have fixed the green body composition, varying some key process parameters, such as firing temperature (T_f), firing time (t_f) and quartz grain size (d_{50}); a grid of 30 T_f–t_f–d_{50} points has been explored. We have spanned the t_f–T_f space (0–80 min; 1200–1280 °C) using firing temperatures representative of the plateau values of the heating curve in industrial processes. X-ray powder diffraction has been used to determine the phase composition for each T_f–t_f–d_{50} point. Scanning electron microscopy proved useful in enhancing the micro-structural characterization. Quartz d_{50} seems to be the process-parameter which most effectively co-relates with the thermal expansion of the glassy matrix.

Keywords: Firing; Traditional ceramics; X-ray methods; Water absorption; Thermal expansion

1. Introduction

It is common industrial practice to assess the quality of a ceramic body for sanitary-ware through macroscopic measurements which are representative either of its processability or of its response to fatigue.[1] This is dependent on the phases and their micro-structures that have developed during firing, as a function of the initial raw materials and of a set of key process parameters, which, in turn, influence the thermodynamic solid state reactions leading to a finite ceramic body.[1–3] In such a view, understanding the connection between process parameters, the observed phases and the physical properties of a fired body is a step towards a full rationalization of the industrial production cycle.

The general aim of the present work is to contribute to understanding the relationships between peak firing-temperature (T_f), firing-time (t_f), quartz particle size (d_{50}), phase-contents developed upon heating, and two macroscopic properties that are important to the pre-production assessment of a casting slip: thermal dilatation and water absorption of the related ceramic body. Thermal dilatation and water absorption are strongly connected with the processability of a body, the former governing its shrinkage upon cooling, and the latter providing a quantification of a crucial property for vitreous sanitary-ware. Earlier studies have shed light on how the quartz content and its particle grain size influence the mechanical properties of a finite ceramic body.[4]

A blend of kaolin, clay, Na-feldspar and quartz (d_{50} ∼18 and ∼50 μm), used to mimic a prototypical industrial slip, was fired at 1200, 1240, 1280 °C for 0–20–40–60–80 min. The fired ceramic pieces thus obtained have been studied by: (i) X-ray powder diffraction to quantify the phases occurring; (ii) scan-

* Corresponding author. Tel.: +39 02 503 15621; fax: +39 02 503 15597.
E-mail address: valeria.diella@idpa.cnr.it (V. Diella).

0955-2219/$ – see front matter © 2011 Elsevier Ltd. All rights reserved.
doi:10.1016/j.jeurceramsoc.2011.02.006

ning electron microscopy to investigate some aspects of their micro-structures; (iii) thermal dilatometry to determine the thermal expansion coefficient; and (iv) water absorption to quantify the degree of interconnected porosity, in a way relevant to the industrial assessment of a sanitary-ware product. The phase composition and the macroscopic observables have then been related to T_f, t_f and quartz-d_{50}.

2. Experimental

2.1. Samples

The green body was obtained mixing with a flunger in wet conditions commercial raw materials in the ratio: 27 wt% kaolin, 23 wt% ball clay, 25 wt% Na-feldspar and 25 wt% quartz (d_{50} ∼18, ∼25 and ∼50 μm). Their elemental composition is shown in Table 1. Given that the results obtained using quartz with d_{50} ∼18 and ∼25 μm were identical within experimental uncertainty, we have chosen to focus our discussion on the cases of d_{50} ∼18 and ∼50 μm, *i.e.* those which best bring to light the effects due to the average quartz particle size.

The slip was aged for 24 h, cast into cylinders with diameter and length of 0.8 and 6 cm, respectively, then fired according to the t_f–T_f grid of Table 2 and eventually quenched to room temperature. Firing was performed in a static kiln, setting the heating ramp at 10 °C/min. 3–4 Samples at each t_f–T_f–d_{50} point allowed assessment of the reproducibility of the results and reduction, through averaging, of noise due to statistical variation.

2.2. X-ray powder diffraction (XRPD)

Samples cut from the fired cylinders and manually ground in an agate mortar, were examined by X-ray powder diffraction, using an X'Pert Panalytical Diffractometer, in θ–2θ Bragg-Brentano geometry, equipped with an X'Celeretor Detector. A 2θ range of 10–70° (Cu Kα-radiation, 40 kV, 40 mA) was explored with a stepsize of 0.02° and a counting time of 30 s/step.

The glass content of sanitary-ware ceramic bodies was determined following the commonly used method of Gualtieri,[5] which relies upon an addition of 20 wt% high-purity calcined α-Al_2O_3 (ICSD 10425) serving as an internal standard for re-scaling the phase contents predicted by Rietveld treatment.[6,7] The quartz content was also cross-checked, by a re-determination performed using the Reference Intensity Ratio (R.I.R.) technique.[8] The powder diffraction patterns were processed using the GSAS software package.[9] The 2θ-intensity profiles were modelled using pseudo-Voigt functions[6]; for each phase, the relative scale factor, cell parameters, profile width parameters, preferred orientation coefficient after March–Dollase[10] were refined. Twelve coefficients were used to describe the background in terms of a Chebyshev polynomial series.

2.3. Scanning electron microscopy (SEM)

All samples were analyzed using a Cambridge Stereoscan 360 scanning electron microscope to investigate their phase-morphology and micro-structural features, and to discriminate between primary and secondary mullite crystals. The cylinders were cut transversally into 5 mm thick slices with a water-lubricated rock saw. Discrimination between primary and secondary mullite requires removal of as much of the glassy matrix embedding the crystals as possible. This was accomplished by etching the samples' surface by means of flouro-boric acid, which is an effective method for dissolving part of the glassy matrix, allowing an improved view of the crystals trapped inside.

2.4. Thermal expansion

Thermal dilatation measurements were carried out using a Netzsch Dilatometer 402 ED, previously calibrated on alumina and tested for industrial sanitary-ware samples, setting the temperature ramp rate at 5.5 °C/min. The sample length was recorded every 0.1 min, between 20 and 815 °C.

The linear thermal expansion coefficient (α_L) and the sample length at temperature T, *i.e.* $L(T)$, are related to one another via the expression beneath

$$L(T) = L_0 \exp[\alpha_L(T - T_0)]$$

where the subscript 0 indicates ambient conditions; α_L is here modelled by a constant term.

The volume (V) thermal expansion coefficient (α) of bodies consituted of more than one phase (a subscript j is hereafter used to attribute a given quantity to the jth-phase) can be expressed as:

$$\alpha = \frac{1}{V} \times \left(\frac{\partial V}{\partial T}\right) = \frac{1}{[\Sigma_j V_j(T)]} \times \left[\frac{\partial \Sigma_j V_j(T)}{\partial T}\right] \quad (1)$$

Eq. (1) can readily be cast into

$$\alpha = \frac{[\Sigma_j \lambda_j \times \alpha_j/\rho_j]}{\Sigma_j \lambda_j/\rho_j} \quad (2)$$

where λ_j and ρ_j are the weight fraction and density of the jth-phase, respectively. We use for λ_j, ρ_j and α_j their values at room conditions, which provide an excellent approximation for the present case, but for the volume thermal expansion coefficient of quartz, for which we adopted its average value on the 25–550 °C T-range.

Note that: (i) in isotropic bodies the relationship between linear and volume thermal expansion coefficients is $\alpha \approx 3 \times \alpha_L$; (ii) the model of Eq. (1) neglects the effects due to the contact surfaces between phases; (iii) $\rho_{glass} \sim 2.07\ g\ cm^{-3}$, as used here, is an estimation resulting from an average based on over 50 picnometer density measurements of ceramic bodies, where the raw ρ-values had been properly corrected to account for the embedded crystal phases.

2.5. Water absorption

The water absorption coefficient (WA) was determined using the following procedure: the sample was dried for 12 h at 110 °C and its weight (m_d) measured using an analytical balance; the sample was then immersed in water and boiled for 2 h, cooled

Table 1
Elemental composition of the raw materials used for the initial slip composition. Average uncertainly about 1%.

Wt%	Raw material (industrial name)	Chemical composition (wt%)							
		SiO_2	Al_2O_3	Fe_2O_3	MgO	TiO_2	CaO	K_2O	Na_2O
27	Kaolin	54.25	41.82	1.08	0.34	0.06	0.08	2.26	0.17
23	Clay minerals	55.65	39.52	1.38	0.23	1.04	0.23	1.73	0.23
25	Quartz	99.42	0.4	0.05	0	0	0.02	0.05	0.05
25	Feldspar	71.29	18.07	0.13	0.1	0.06	0.2	0.10	10.04

in situ for 12 h and re-weighed (m_w). Hereafter, we use the WA coefficient calculated as:

$$WA = \left[\frac{(m_w - m_d)}{m_d}\right] \times 100.$$

This parameter is commonly adopted in the industrial practice to quantify the degree of porosity, and assess whether the finished sanitary-ware bodies meet the technical requirements.

3. Results and discussion

3.1. Phase evolution versus t_f–T_f–d_{50}

In Table 2 we report the phase compositions developed at each t_f–T_f–d_{50} point, determined as the average of 3–4 independent experimental runs at the same time–temperature–quartz size conditions. We adopt the acronyms SM and S2 to refer to the sample series obtained using quartz raw materials of d_{50} ~18, and ~50 μm, respectively.

Fig. 1 shows the phase evolution as a function of t_f and T_f, for the samples of the SM and S2 series.

Preliminary qualitative XRPD-measurements have shown the occurrence of quartz (ICSD 67117), mullite (ICSD 100805) and glass in all samples, along with Na-feldspar (ICSD 87654) only in specimens fired at 1200° and 1240 °C, and t_f = 0 min (*i.e.* at the end of the heating ramps). Kaolinite and clay minerals are completely absent following such thermal a treatment, as their decomposition reactions[2] take place at a lower temperature, and promote the formation of mullite and Si–Al-rich glass. Fig. 2 shows the Rietveld plot of sample S2 fired at 1200 °C for 0 min with α-Al_2O_3 added as internal standard.

Table 2
Mineralogical composition (wt%) of the samples after firing. Estimated accuracy on the basis of repeated measures is ~0.5% to 0.8%. α_L is the linear expansion coefficient over the interval 30–540 °C.

t_f (min)	T_f (°C)	d_{50} (μm)	Mullite	Quartz	Feldspar	Glass	W.A.	α_L ($\times 10^{-6}$ °C^{-1})
0	1200	50	14.9	28.6	10.5	46.0	9.5	5.16
20	1200	50	19.4	27.7	3.8	49.1	3.6	5.00
40	1200	50	17.5	27.2	2.4	52.9	4.1	5.04
60	1200	50	18.3	25.3	2.4	54.0	2.4	5.20
80	1200	50	17.0	25.7	2.1	55.2	2.7	5.16
0	1240	50	16.5	28.3	3.4	51.8	5.4	5.07
20	1240	50	18.0	26.7	0.0	55.3	3.7	5.56
40	1240	50	17.7	23.6	0.0	58.7	1.6	5.32
60	1240	50	18.0	22.6	0.0	59.4	1.1	5.58
80	1240	50	19.5	21.4	0.0	59.1	1.0	5.42
0	1280	50	17.4	24.2	0.0	58.4	3.6	5.24
20	1280	50	17.7	24.1	0.0	58.2	1.7	5.31
40	1280	50	17.6	22.3	0.0	60.1	1.6	5.23
60	1280	50	17.6	19.9	0.0	62.5	0.7	5.03
80	1280	50	17.6	19.5	0.0	62.9	0.5	5.01
0	1200	18	16.1	27.1	8.4	48.4	10.2	5.11
20	1200	18	17.9	24.0	2.4	55.7	3.7	5.83
40	1200	18	18.1	22.3	2.3	57.3	2.7	5.17
60	1200	18	17.2	20.3	1.5	61.0	2.0	6.24
80	1200	18	17.0	17.9	0.8	64.3	0.8	5.44
0	1240	18	17.8	24.7	3.5	54.0	5.6	5.60
20	1240	18	17.3	19.8	0.0	62.9	0.9	5.79
40	1240	18	17.6	18.7	0.0	63.7	0.8	6.17
60	1240	18	17.1	16.3	0.0	66.6	0.6	5.94
80	1240	18	17.5	15.0	0.0	67.5	0.4	5.62
0	1280	18	18.2	21.8	0.0	60.0	2.8	5.42
20	1280	18	17.6	18.5	0.0	63.9	0.7	5.49
40	1280	18	16.8	14.3	0.0	68.9	0.4	4.89
60	1280	18	16.9	13.9	0.0	69.2	0.3	5.12
80	1280	18	16.4	13.0	0.0	70.6	0.3	5.63

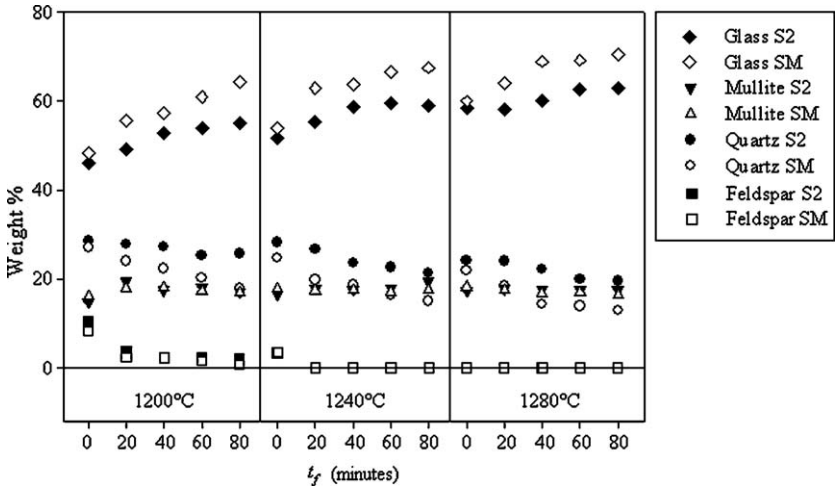

Fig. 1. Phase content evolution as a function of t_f, T_f and d_{50}.

Quartz reactivity can be related to d_{50}, as proven by comparing the quartz contents in samples at $t_f = 0$ min[2,11,12] and same T_f. In discussing the behaviour and role of SiO_2 in the materials on study, it is important to take into account that the complex silica phase diagram as a function of temperature depends both on the heating/cooling rate of the thermal treatment[13,14] and on the parent slip's phase composition. Crystalline Na-feldspar was observed above its conventional temperature range of stability, presumably because of kinetics[2]: at larger t_f-values, for $T_f = 1240\,^{\circ}C$, it had definitely disappeared.

The full slopes [$\varphi_{full}(X)$, where X: quartz, mullite and glass] and partial slopes [$\varphi_y(X)$, where X: quartz, mullite and glass; y: (*a*) 0–40 and (*b*) 40–80 min ranges] of the phase content curves as a function of t_f, at given T_f, are set out in Table 3 and used to help elucidate the roles of firing parameters and quartz particle size distribution in the formation of the final phases.[15] It may be concluded that:

1. Mullite content does not appreciably increase as a function of t_f (as shown in Fig. 1 and Table 2). This suggests that the mullite formation reaction is largely completed during the heating ramp at least on the timescale employed industrially. Neither quartz grain size, nor T_f, seem significantly to affect the rate of mullite formation, which varies between 15–19 and 16–18 wt% in S2 and SM, respectively, at $t_f > 0$. Mullite begins to form at about 1000 °C influenced by clay and feldspar presence,[2,16,17] and at the end of the heating ramp the resulting multi-phase system achieves an "equilibrium-like" condition without further significant phase-changes, save probably over a longer timespan than that examined.
2. Comparing $\varphi_{0–40}(quartz)$ versus $\varphi_{40–80}(quartz)$, and $\varphi_{0–40}(glass)$ versus $\varphi_{40–80}(glass)$ indicates that most reactions involving phase-formation take place during the first 40 min of firing. This is particularly evident for the samples treated at 1240 and 1280 °C, indicating a higher rate of

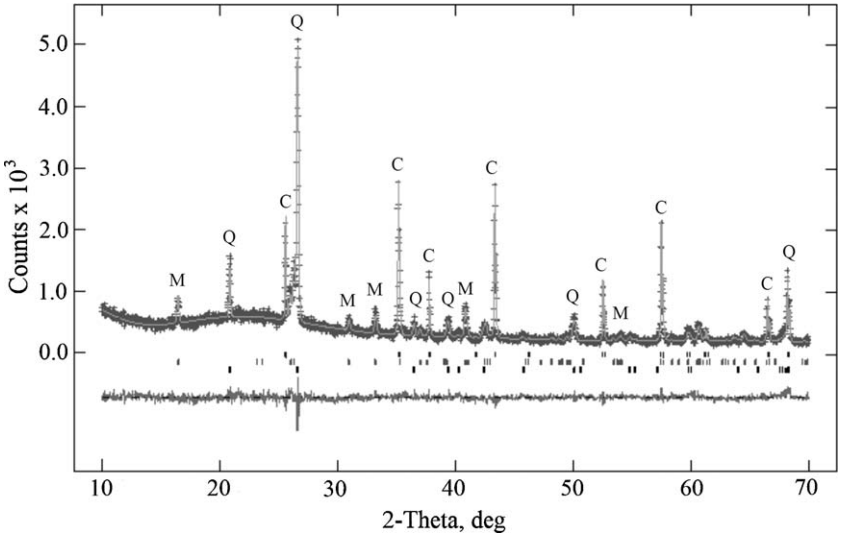

Fig. 2. Rietveld plot for sample S2 fired at 1200 °C for 0 min with α-corundum added as internal standard. Peak labels are Q for quartz, M for mullite, A for albite and C for corundum.

Table 3
Full (0–80 min) and partial (0–40 min; 40–80 min) slopes of phases-contents versus t_f in fired bodies. x and y are the ends of the interval over which the slopes are calculated.

T_f (°C)	S2 (0–80 min)	S2 (0–40 min)	S2 (40–80 min)	SM (0–80 min)	SM (0–40 min)	SM (40–80 min)
$\varphi_{x-y}(quartz)$ (min^{-1})						
1200 °C	−0.04	−0.03	−0.04	−0.11	−0.12	−0.11
1240 °C	−0.08	−0.12	−0.05	−0.11	−0.15	−0.9
1280 °C	−0.07	−0.05	−0.07	−0.11	−0.19	−0.03
$\varphi_{x-y}(glass)$ (min^{-1})						
1200 °C	0.12	0.17	0.06	0.19	0.22	0.18
1240 °C	0.09	0.17	0.01	0.15	0.24	0.10
1280 °C	0.07	0.04	0.07	0.13	0.22	0.04
$\varphi_{x-y}(mullite)$ (min^{-1})						
1200 °C	0.02	0.07	−0.01	0.01	0.05	−0.03
1240 °C	0.03	0.03	0.04	0.00	−0.01	0.00
1280 °C	0.00	0.01	0.00	−0.02	−0.04	−0.01

reaction at higher T_f. Moreover, this is seen more clearly in the SM-series than S2, which emphasizes the role of the quartz grain size in reactivity, *i.e.* the smaller d_{50}(quartz), the larger its rate of reaction.

3. No trydimite was observed; although thermodynamically favoured, its formation is kinetically impeded except in the presence of specific promoters[18,19]; similarly, cristobalite, which forms in situ at even lower T_fs starting from pure glass precursors but fails to survive cooling.[2]

3.2. Micro-structures

All samples were inspected by scanning electron microscope to investigate the evolution of the micro-structures developed during firing. Fig. 3 shows six examples. A widespread lamellar habit was observed in the samples at the end of a heating ramp, *i.e.* $t_f = 0$ min. Given that evidence from the diffraction measurements eliminates any possible clay–mineral, we are inclined to believe this habit relates to the persistence of a residual sheet-mineral-like morphology, whose structure arrangement is no longer that of the parent phyllosilicate, which has utterly lost the peculiarity of long-range order.

As shown in Fig. 3, the degree of surface homogeneity appears to increase as a function of t_f and T_f; the lamellar habit progressively changes into flakes, which are not seen at the highest temperatures. Backscattered electron images allow one to observe the distribution of primary and secondary mullite,[16,17] the former assuming a "cuboidal" habit, the latter an elongated one (Fig. 4). It would seem that primary mullite is more abundant than secondary in the samples fired up to 40 min and 1240 °C; a remarkable increase of secondary mullite is apparent in the samples heated for 80 min at 1280 °C.

3.3. Water absorption

WA measurements show a marked decrease of the water absorption parameter as a function of firing time and temperature, and this trend is more visible in the SM-series. At the end of each heating ramp, SM and S2 exhibit similar WA-values, which diverge upon further firing. In Fig. 5, WA is displayed with respect to t_f and T_f. In general, the trends seem to reflect a vitrification process that proceeds monotonically as a function of t_f, and is accelerated in samples having smaller quartz grains. Focussing on series SM, a more detailed inspection of Fig. 5 reveals a remarkable sensitivity of WA to T_f and t_f: in particular, passing from 1200 to 1240 and then to 1280 °C, one realises that WA approximately halves for a 40 °C increase in T_f. A WA of 0.5% is a typically accepted value for a fired body destined for sale; this is achieved in SM at 1240 °C after 20 min, but in S2 only at 1280 °C and after 80 min. For the same glass content, WA is systematically larger in SM than S2. Equal glass amounts in SM and S2 were obtained by increasing t_fs for S2. The importance of firing time suggests that its role cannot only be promotion of glass formation, but may also involve formation of specific micro-structures. The role of t_f is stressed in Table 4, in which we report the partial WA contributions over two different t_f ranges, calculated as:

$$\frac{[WA(t_{f,1}, T_f) - WA(t_{f,2}, T_f)]}{[WA(t_{f,m}, T_f) - WA(t_{f,M}, T_f)]} \times 100,$$

where $t_{f,m} = 0$ s, $t_{f,M}$ is the largest t_f value used and $t_{f,m} \le t_{f,1} < t_{f,2} \le t_{f,M}$.

It was seen that over the first 40 min the average WA decreased by ∼77.5% in S2, but by ∼89.5% in SM.

3.4. Thermal expansion

Fig. 6 shows a typical thermal dilatation curve for a ceramic sanitary-ware body. The curve can be divided into three temperature ranges: the first trails linearly from room conditions to ∼550 °C; the second, from 550 to 600 °C, is substantially governed by the α–β quartz displacive phase transition; the last, above 600 °C, is reflective of a variety of transformations involving the glass phase.[20] We focus here on the first range, which is the most significant to the shrinkage of a sanitary-ware body on steady cooling.

The volume thermal expansion of a ceramic sanitary-ware body (α_{CB}) over the thermal range up to 550 °C has been mod-

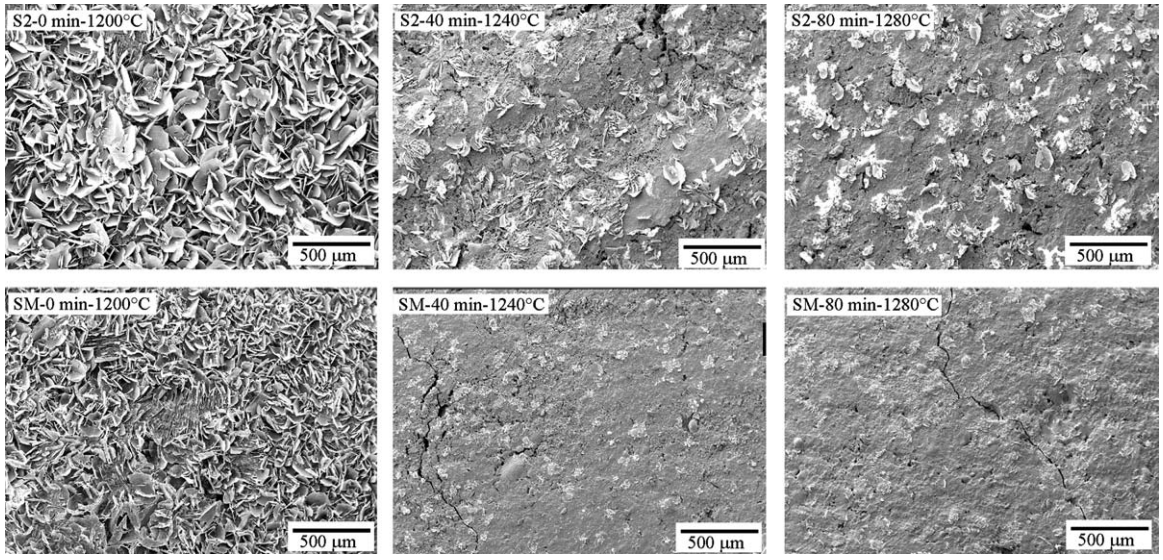

Fig. 3. Backscattered electrons images of the surfaces of ceramic bodies treated at different firing temperatures and firing time conditions.

Table 4
Water absorption contributions in the ranges 0–40 and 40–80 min.

T_f (°C)	S2 (0–40 min)	S2 (40–80 min)	SM (0–40 min)	SM (40–80 min)
1200 °C	80.44%	19.56%	80.35%	19.65%
1240 °C	86.96%	13.04%	92.04%	7.96%
1280 °C	64.94%	35.06%	96.07%	3.93%
Mean value	77.45%	22.55%	89.49%	10.51%

elled by Eq. (2), using the literature values[21] for the volume thermal expansion coefficients of quartz (mean value over the explored T-range, *i.e.* $48.9 \times 10^{-6}\,^{\circ}C^{-1}$), feldspar and mullite, and parameterising that of glass as:

$$\alpha_{glass} = \alpha_0 + \alpha_1 \times (T_f - 1200\ ^{\circ}C) + \alpha_2 \times t_f + \alpha_3 \times d_{50}. \quad (3)$$

The coefficients α_0, α_1, α_2 and α_3 have been determined by a minimization of the differences between observed and theoretical α_{CB}-values. The 1200 °C in Eq. (3) was introduced to emphasize the difference between the three T_fs examined. α_3 is meant to account for micro-structuring of glass around quartz crystals; this process is expected to be sensitive to the grain size, *i.e.* d_{50}. In so doing, one attains the results set out in Table 5, which yield an average volume thermal expansion coefficient for glass of $6.36 \times 10^{-6}\,^{\circ}C^{-1}$. This figure is in keeping with those from[22] and references therein, which refer to silica-based glasses. We investigated the effect due to the co-relations between the α_0, α_1, α_2 and α_3 parameters by varying sub-sets of them in the minimization runs; in so doing, we observed that the percentage contribution of each (i) does not change significantly and (ii) preserves its sign. Table 5 shows that α_0 and α_3 are the main contributors to α_{glass}, whereas α_1 affects the volume thermal expansion coefficient of the amorphous phase more modestly. Fig. 7 clearly indicates the important role of d_{50} in affecting the dilatation behaviour of sanitary-ware bodies. The quartz content in the S2 samples is systematically higher than in SM, which is somewhat contradictory with expectation, as S2

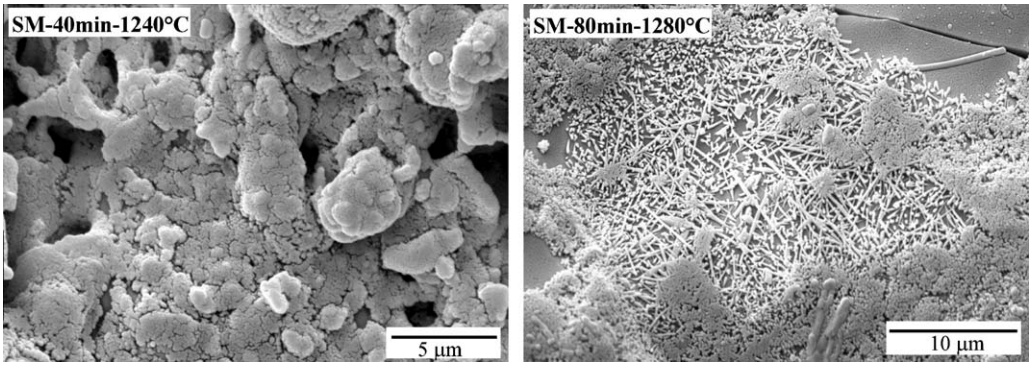

Fig. 4. Backscattering electrons images of mullite crystals formed in the ceramic bodies on study. Samples etched with BF_4H.

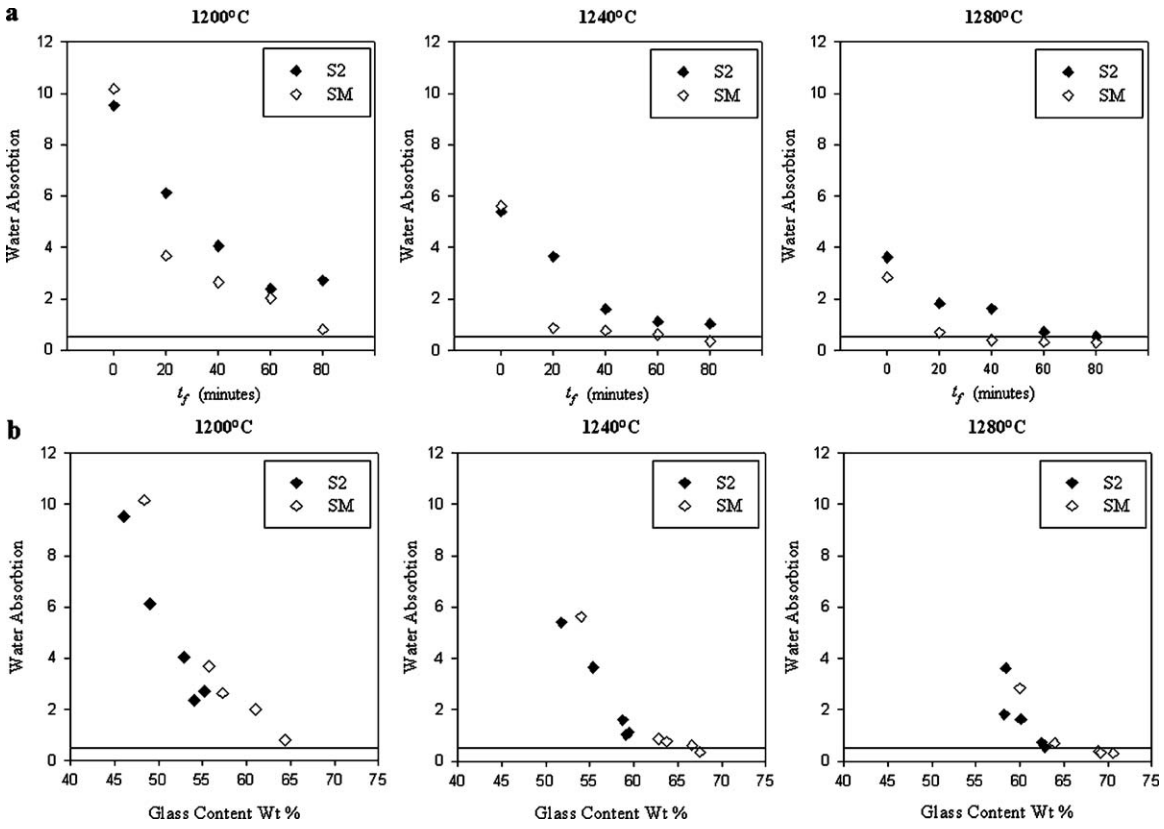

Fig. 5. Water absorption values as a function of t_f (a) and of the glass-phase amount (b), for the SM- and S2-series. The horizontal line (WA = 0.5) indicates the typically accepted WA-value for a sanitary-ware body.

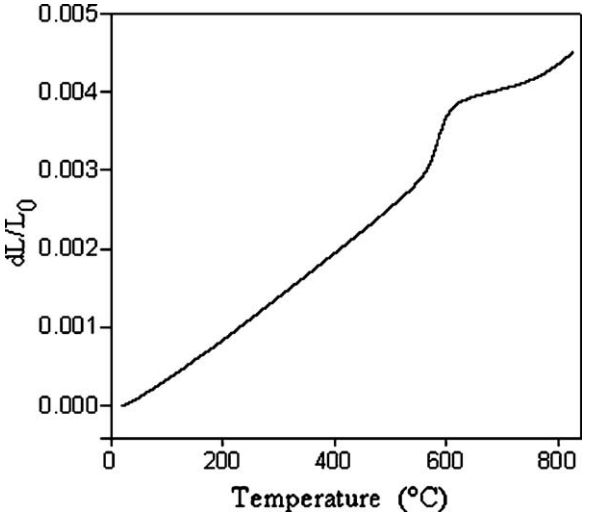

Fig. 6. Classic thermal dilatation curve for a sanitary-ware ceramic body over the range 25–820 °C.

has a smaller value of α_{CB}s. The negative sign of α_3 confirms a tendency to reduce the dilatation of a sanitary-ware body as size of the quartz grains increases. We believe such behaviour may be ascribed to the interface between the quartz and the glass matrix, which may act as a "cushion", partially compensating for the dilatation of quartz, the most expansive of the minerals occurring in the ceramic body. This mechanism might be enacted through detachments of the glassy matrix from the quartz surface, and/or complex micro-structural arrangements of the glass phase in the vicinity, both favoured by the large continuous surfaces of big quartz grains.

t_f affects the volume thermal expansion via the α_2-coefficient, suggesting that increased firing time leads to a more expansive body. The longer t_f, the lower the quartz content. This is again in conflict with the commonly held notion that thermal dilatation is mainly controlled by the amount of quartz, and supports the hypothesis that micro-structures in the amorphous matrix, dependent on the firing duration, significantly affect α_{glass}, in keeping with.[23–26]

Table 5
Glass thermal expansion coefficient, according to Eq. (3) of the text.

25–550 °C	α_0 ($\times 10^{-6}$ °C^{-1})	α_1 ($\times 10^{-6}$ °C^{-1})	α_2 ($\times 10^{-6}$ °C^{-1})	α_3 ($\times 10^{-6}$ °C^{-1})	$\langle\alpha_{glass}\rangle$ ($\times 10^{-6}$ °C^{-1})
Coefficient value	6.711	0.041	0.071	−0.147	6.36
Contribution % to the total α-value	105	25	43	−75	–

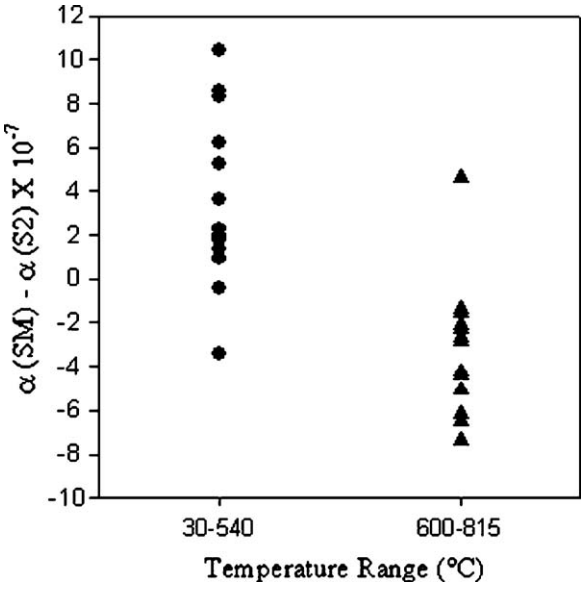

Fig. 7. Linear thermal expansion coefficient of ceramic sanitary-ware bodies as a function of d_{50}.

4. Conclusions

1. The process parameters t_f–T_f–d_{50} have a remarkable role in affecting the evolution of the phases, as shown by the slopes of the phase-content versus firing-time curves, reported in Table 3.
2. In general, the SM series (*i.e.* quartz $d_{50} \sim 18\,\mu m$) exhibits a higher rate of phase-transformation than S2 (quartz $d_{50} \sim 50\,\mu m$).
3. A tendency to develop secondary mullite upon increasing T_f and t_f is seen in keeping with the complete collapse of the feldspar structures.
4. The size of the quartz grains affects the water absorption coefficient: the finer d_{50} (for the same t_f and T_f), the smaller WA.
5. t_f is a crucial parameter in the promotion of vitrification; decreasing water absorption follows increasing t_f.
6. The volume thermal expansion coefficient of glass is significantly affected by d_{50}, to a lesser extent by t_f, and in a minor way by T_f, within the scope of the range of the process parameters space examined. The average α_{glass}-value measured is $6.36 \times 10^{-6}\,^{\circ}C^{-1}$, corresponding to an average linear thermal expansion coefficient of $2.07 \times 10^{-6}\,^{\circ}C^{-1}$.

References

1. Barbieri L, Bonfatti L, Ferrari AM, Leonelli C, Manfredini T, Settembre D. Relationship between microstructure and mechanical properties in fully vitrified stoneware. In: Vincenzini P. editor. *Techna SrL*; 1995. p. 99–105.
2. Carty WM, Senapati U. Porcelain: raw materials, processing, phase evolution and mechanical behaviour. *J Am Ceram Soc* 1998;**81**:3–20.
3. Lee WM, Rainforth WM. *Ceramic microstructure*. UK: Chapman & Hall; 1995.
4. Hamano K, Wu YH, Nakagawa Z, Hasegawa M. Effect of grain size of quartz on mechanical strength of porcelain bodies. *J Ceram Soc Jpn* 1991;**99**:153–7.
5. Gualtieri AF. Accuracy of XRPD QPA using the combined Rietveld-RIR method. *J Appl Crystallogr* 2000;**33**:267–78.
6. McCusker LB, Von Dreele RB, Cox DE, Louer D, Scardi P. Rietveld refinement guidelines. *J Appl Crystallogr* 1999;**32**:36–50.
7. Young RA. *The Rietveld method*. Oxford: University Press; 1993.
8. Chung FH. Quantitative interpretation of X-ray diffraction patterns of mixtures. I. Matrix-flushing method for quantitative multicomponent analysis. *J Appl Crystallogr* 1974;**7**:519–25.
9. Larson AC, Von Dreele RB. *General Structure Analysis System (GSAS)*. Los Alamos Natl. Lab Rep. LAUR; 2004. p. 86–748.
10. Dollase WA. Correction of intensities for preferred orientation in powder diffractometry: application of the March model. *J Appl Crystallogr* 1986;**19**:267–72.
11. Martin-Marquez J, De la Torre A, Aranda MAG, Rincon JM, Romero M. Evolution with temperature of crystalline and amorphous phase in porcelain stoneware. *J Am Ceram Soc* 2009;**92**:229–34.
12. Iqbal Y, Lee WE. Microstructural evolution in triaxial porcelain. *J Am Ceram Soc* 2000;**83**:3121–7.
13. Haney PH. Structure and chemistry of the low-pressure silica polymorphs. In: *Reviews in mineralogy. Physical behavior, geochemistry and materials applications*, vol. 29;1. Washington, DC: Mineralogical Society of America; 1994. p. 1–40.
14. Ackermann RJ, Sorrell CA. Thermal expansion and the high-low transformation in quartz. *J Appl Crystallogr* 1974;**7**:461–7.
15. Stathis G, Ekonomakou A, Stournaras CJ, Ftikos C. Effect of firing conditions, filler grain size and quartz content on bending strength and physical properties of sanitaryware porcelain. *J Eur Ceram Soc* 2004;**24**:2357–66.
16. Lee WE, Souza GP, McConville CJ, Tarvornpanich P, Iqbal Y. Mullite formation in clays and clay-derived vitreous ceramics. *J Eur Ceram Soc* 2008;**28**:465–71.
17. Martin-Marquez J, Rincòn JM, Romero M. Mullite development on firing in porcelain stoneware bodies. *J Eur Ceram Soc* 2010;**30**:1599–607.
18. Moroz M, Maslennikova GN, Mironova AF, Platov YP. *Formation of tridymite and cristobalite from quartz in porcelain. Glass and ceramic*, vol. 37;3. Springer; 1980. p. 147–50.
19. Tarvornpanich T, Souza GP, Lee WE. Microstructural evolution in clay-based ceramics II: ternary and quaternary mixtures of clay, flux and quartz filler. *J Am Ceram Soc* 2008;**91**:2272–80.
20. Stillinger FH. Supercooled liquids, glass transitions, and the Kauzmann paradox. *J Chem Phys* 1988;**88**:7818–25.
21. Fei Y. Thermal expansion. In: Ahrens TJ. editor. *Mineral physics and crystallography: a handbook of physical constants*, vol. 2. AGU Reference Shelf; 1995.
22. Fluegel A. Thermal Expansion Calculation of Silicate Glasses at 210 °C, Based on the Systematic Analysis of Global Databases. http://glassproperties.com (December 2007).
23. Scholze H. *Glass – nature, structure and properties*. Springer-Verlag; 1991.
24. Mazurin OV, Porai-Koshits EA, editors. *Phase separation in glass*. Amsterdam, New York: Elsevier Science Publishers B.V., North-Holland; 1984.
25. Simmons JH, Uhlmann DR, Beall GH. editors. *Nucleation and crystallization in glasses. "Advances in ceramics"*, vol. 4. Columbus, OH: The American Ceramic Society; 1982.
26. Stozharov AI, Bogatyreva VV. The thermal expansion coefficient and the stability of the refractive index of glasses. *Sov J Opt Technol* 1975;**42**:595.